



Pulsed optical parametric amplification in chiral media

FREDRIK JONSSON,^{1,2,*} CHRISTOS FLYTZANIS,³ AND GOVIND P. AGRAWAL⁴

¹Division of Electricity, Department of Electrical Engineering, Uppsala University, SE-751 03 Uppsala, Sweden

²Mycronic AB, SE-183 03 Täby, Sweden

³Laboratoire de Physique de l'École Normale Supérieure, ENS, Université PSL, CNRS, Sorbonne Université, Université Paris Cité, F-75005 Paris, France

⁴The Institute of Optics, University of Rochester, Rochester, New York 14627, USA

*fredrik.jonsson@angstrom.uu.se

Received 3 April 2025; revised 1 May 2025; accepted 1 May 2025; posted 6 May 2025; published 23 May 2025

We discuss how the chirality of a nonlinear medium affects the process of optical parametric amplification when optical pulses are used for the pump and signal waves. A set of six coupled nonlinear equations is derived for the circularly polarized components of the pump, signal, and idler pulses, after including the electric dipolar and chiral contributions to the linear and nonlinear susceptibilities of the medium. Our equations include differential group delay and group-velocity dispersion between orthogonal circular polarization states, introduced by the chirality. The Manley–Rowe relations for the pulsed nonlinear process are presented, including their corrections due to nonlocal interactions imposed by the chirality. Numerical solutions reveal novel features such as the possibility of fast intrapulse polarization state flipping and differential phase-matching. © 2025 Optica Publishing Group. All rights, including for text and data mining (TDM), Artificial Intelligence (AI) training, and similar technologies, are reserved.

<https://doi.org/10.1364/JOSAB.563862>

1. INTRODUCTION

In optical parametric amplification (OPA) [1], three waves interact within a nonlinear medium in such a way that a continuous exchange of energy occurs between the pump, signal, and idler waves. When a pair of pump and signal beams, of angular frequencies ω_3 and ω_2 , respectively, is launched into the nonlinear medium, the parametric process allows for an amplification of the signal, meanwhile generating an idler wave at angular frequency $\omega_1 = \omega_3 - \omega_2$. In a setup involving optical pulses, not only does the classical phase-matching [2] come into play but also the different group velocities and dispersion-induced broadening of the three pulses. Just to mention a few examples, quasi-phase-matching [3], chirped-pulse amplification [4], and soliton pulse compression [5] have been used for balancing the mismatch among phases and group velocities of pulses involved in the OPA process. In this respect, a chiral medium presents an interesting opportunity by providing differential additions to the phase and group velocities of orthogonal circular polarizations [6–8].

The differential aspect of phase and group velocities in a chiral medium originates from an interplay between light and matter described by the semi-classical interaction Hamiltonian $\hat{H}_I = -(\hat{p}_j E_j + \hat{Q}_{ij} \partial E_j / \partial x_i)$, where \hat{p}_j and \hat{Q}_{ij} are the quantum-mechanical local electric dipolar and nonlocal electric quadrupolar operators acting in a classical field E_j [9]. Additionally, the nonlinear coupling coefficients between

the pump, signal, and idler waves are also modified in a chiral medium to include nonlocal effects. The differential nonlocal corrections to orthogonal circularly polarized modes in a nonlinear optical regime are expressed as functions of the magnitude of the respective wave vectors. These corrections act on the amplitudes of the fields, besides the differential correction terms for their phase.

Of particular interest for such chiral effects are crystals of point-symmetry group 23 (cubic) and 32 (trigonal, uniaxial), which exhibit isotropic behavior when rotated around their z axis. Not possessing any center of inversion, these crystals exhibit the required chirality as well as second-order optical susceptibilities supporting parametric interaction. Examples of other media that satisfy this criterion are nematic liquid crystals [10,11] and optically active sodium bromate [12,13].

In this work, we discuss the impact of chirality on the OPA process when the pump, signal, and idler waves are supplied as optical pulses. Section 2 presents the linear and nonlinear contributions to the electric polarization density in a chiral nonlinear medium, which are used in Section 3 to obtain a set of six coupled nonlinear equations for the circularly polarized components of the three pulses. Our equations explicitly include the differential group delay and group-velocity dispersion between these two components, induced by the chirality. This set of equations is solved numerically in Section 4 to study the OPA process with emphasis on changes in the state of polarization. The main results are summarized in Section 5.

2. LINEAR AND NONLINEAR CONTRIBUTIONS

To simplify the problem, we consider three planar quasi-monochromatic fields co-propagating along the z axis inside a medium of point-symmetry group 32. When expressed in a left/right circularly polarized (LCP/RCP) basis with basis vectors $\mathbf{e}_\pm = (\mathbf{e}_x \pm i\mathbf{e}_y)/\sqrt{2}$, the total electric field can be written as

$$\mathbf{E}(z, t) = \sum_{j=1}^3 \text{Re}[(\mathbf{e}_+ E_{\omega_j}^+(z, t) + \mathbf{e}_- E_{\omega_j}^-(z, t)) \exp(-i\omega_j t)], \quad (1)$$

with $j = 1, 2, 3$ designating the idler, signal, and pump waves, respectively, whose frequencies satisfy the condition $\omega_1 + \omega_2 = \omega_3$ for the OPA process.

As point-symmetry group 32 does not possess a center of inversion, the axial tensor γ_{ijkl} for nonlocal and nonlinear interaction shares the same nonzero and independent elements as the third-order polar tensor χ_{ijkl} for local (electric dipolar) interactions [9]. In this situation, the electric polarization density of the medium for the LCP and RCP states takes the form [6, 14]

$$P_{\omega_{1,2}}^\pm = \varepsilon_0 \left(n_{1,2}^2 - 1 \pm i\gamma_{1,2} \frac{\partial}{\partial z} \right) E_{\omega_{1,2}}^\pm + \varepsilon_0 \left(p_{1,2} \pm iq_{1,2} \frac{\partial}{\partial z} \right) (E_{\omega_3}^\mp E_{\omega_{2,1}}^{\pm*}), \quad (2a)$$

$$P_{\omega_3}^\pm = \varepsilon_0 \left(n_3^2 - 1 \pm i\gamma_3 \frac{\partial}{\partial z} \right) E_{\omega_3}^\pm + \varepsilon_0 \left(p_3 \pm iq_3 \frac{\partial}{\partial z} \right) (E_{\omega_1}^\mp E_{\omega_2}^\mp), \quad (2b)$$

where the coefficients are expressed in terms of the elements of the local (χ_{ij} , χ_{ijk}) and nonlocal (γ_{ijk} , γ_{ijkl}) electric susceptibility tensors in standard notation [2] as

$$\begin{aligned} n_j^2 &= 1 + \chi_{xx}(-\omega_j; \omega_j), & \gamma_j &= \gamma_{xyz}(-\omega_j; \omega_j), \\ p_{1,2} &= 2^{1/2} \chi_{xxx}(-\omega_{1,2}; \omega_3, -\omega_{2,1}), \\ p_3 &= 2^{1/2} \chi_{xxx}(-\omega_3; \omega_1, \omega_2), \\ q_{1,2} &= 2^{1/2} \gamma_{xyz}(-\omega_{1,2}; \omega_3, -\omega_{2,1}), \\ q_3 &= 2^{1/2} \gamma_{xyz}(-\omega_3; \omega_1, \omega_2), \end{aligned} \quad (3)$$

where Kleinman symmetry [9] of the permutation was assumed.

The physical interpretation of the terms in Eq. (2) is as follows. The linear part of the polarization density depends on the refractive indices n_j , originating from the local electric dipolar interaction between light and matter, while the chirality parameter γ_j originates from the nonlocal electric quadrupolar interaction, and where $j = 1, 2, 3$ denotes the idler, signal, and pump wave interactions with the medium, respectively. The second-order nonlinear part depends on p_j and q_j , denoting the local electric dipolar and nonlocal electric quadrupolar contributions, respectively. The nonlinear contribution to the RCP and LCP polarization density at the pump frequency is

exclusively via the pair of LCP and RCP idler and signal fields of opposite polarization state.

3. MODEL FOR WAVE PROPAGATION

In the process of solving Maxwell's equations, it is often convenient to separate the linear and nonlinear contributions to the electric polarization density in Eq. (2) as $P_{\omega_j}^\pm = P_{\omega_j}^{(L)\pm} + P_{\omega_j}^{(NL)\pm}$, where the linear part can be used to define an effective propagation constant, here including nonlocal interactions. To simplify the analysis, for the moment limiting the description to continuous waves, we ignore diffraction effects and apply the plane-wave approximation. Using the form of the electric field in Eq. (1), its LCP and RCP components associated with plane waves propagating along the z axis inside a chiral nonlinear medium satisfy

$$\left(\frac{\partial^2}{\partial z^2} + k_j^2 \pm 2i\alpha_j \frac{\partial}{\partial z} \right) E_{\omega_j}^\pm = -\mu_0 \omega_j^2 P_{\omega_j}^{(NL)\pm}, \quad (4)$$

where the electric dipolar and nonlocal parts of the propagation constants for $j = 1, 2, 3$ are given by

$$k_j = k(\omega_j) = \frac{\omega_j n_j}{c}, \quad \alpha_j = \alpha(\omega_j) = \frac{\omega_j^2 \gamma_j}{2c^2}. \quad (5)$$

Whenever the nonlinear source terms are neglected, Eq. (4) supports forward-propagating solutions in the form

$$E_{\omega_j}^\pm = A_{\omega_j}^\pm \exp(i(k_j \mp \alpha_j)z). \quad (6)$$

By substituting Eq. (6) into Eq. (4), we obtain three frequency-domain equations for the field envelopes associated with the idler, signal, and pump pulses. These can be converted to the time domain after expanding both k_j and α_j around the central frequencies ω_j as Taylor series and retaining terms up to the second order.

Using Eq. (6) as an ansatz for the separation of the spatial natural harmonic oscillation, the time-domain equations for the pulsed envelopes of the LCP and RCP components of three waves, subject to nonlinear interaction within the chiral medium in the presence of group velocity dispersion, are found to yield

$$\begin{aligned} \left(\frac{\partial}{\partial z} + (k'_1 \mp a'_1) \frac{\partial}{\partial t} + \frac{i}{2} (k''_1 \mp a''_1) \frac{\partial^2}{\partial t^2} \right) A_{\omega_1}^\pm \\ = i\kappa_1^\pm A_{\omega_3}^\mp A_{\omega_2}^{\pm*} \exp(i(\Delta k \pm \Delta\alpha)z), \end{aligned} \quad (7a)$$

$$\begin{aligned} \left(\frac{\partial}{\partial z} + (k'_2 \mp a'_2) \frac{\partial}{\partial t} + \frac{i}{2} (k''_2 \mp a''_2) \frac{\partial^2}{\partial t^2} \right) A_{\omega_2}^\pm \\ = i\kappa_2^\pm A_{\omega_3}^\mp A_{\omega_1}^{\pm*} \exp(i(\Delta k \pm \Delta\alpha)z), \end{aligned} \quad (7b)$$

$$\begin{aligned} \left(\frac{\partial}{\partial z} + (k'_3 \pm a'_3) \frac{\partial}{\partial t} + \frac{i}{2} (k''_3 \pm a''_3) \frac{\partial^2}{\partial t^2} \right) A_{\omega_3}^\mp \\ = i\kappa_3^\mp A_{\omega_1}^\pm A_{\omega_2}^\pm \exp(-i(\Delta k \pm \Delta\alpha)z), \end{aligned} \quad (7c)$$

where the first- and second-order electric dipolar dispersion coefficients for the three waves are defined as

$$k'_j = \frac{d}{d\omega} \left(\frac{\omega n(\omega)}{c} \right) \Big|_{\omega_j}, \quad k''_j = \frac{d^2}{d\omega^2} \left(\frac{\omega n(\omega)}{c} \right) \Big|_{\omega_j}, \quad (8)$$

where their respective corrections for the nonlocal interaction in a similar way are defined as

$$a'_j = 2 \frac{d\alpha(\omega)}{d\omega} \Big|_{\omega_j}, \quad a''_j = 2 \left(\frac{d^2\alpha(\omega)}{d\omega^2} - 2k'_j \frac{d\alpha(\omega)}{d\omega k(\omega)} \right) \Big|_{\omega_j}. \quad (9)$$

In Eq. (7), $\Delta k = k_3 - k_2 - k_1$ is the electric dipolar phase mismatch, and $\Delta\alpha = \alpha_1 + \alpha_2 + \alpha_3$ is the nonlocal correction, with nonlinear coupling coefficients

$$\kappa_1^\pm = \frac{k_1}{2n_1^2} [p_1 - q_1(\alpha_3 + \alpha_2) \mp q_1(k_3 - k_2)], \quad (10a)$$

$$\kappa_2^\pm = \frac{k_2}{2n_2^2} [p_2 - q_2(\alpha_3 + \alpha_1) \mp q_2(k_3 - k_1)], \quad (10b)$$

$$\kappa_3^\pm = \frac{k_3}{2n_3^2} [p_3 - q_3(\alpha_1 + \alpha_2) \mp q_3(k_1 + k_2)]. \quad (10c)$$

In these coupling coefficients, p_j are the regular terms, resulting from the electric–dipolar interaction model in a perturbation analysis of the density operator [2], while q_j stems from the nonlocal interaction.

Whenever the group-velocity dispersion, altering the shape and duration of pulses, is negligible compared to the spatial and temporal changes in their amplitudes, Eq. (7) allows for an interpretation of the energy transfer rate between the idler, signal, and pump waves through the relation

$$\begin{aligned} & \frac{1}{\kappa_1^\pm} \left(\frac{\partial}{\partial z} + (k'_1 \mp a'_1) \frac{\partial}{\partial t} \right) |A_{\omega_1}^\pm|^2 \\ &= \frac{1}{\kappa_2^\pm} \left(\frac{\partial}{\partial z} + (k'_2 \mp a'_2) \frac{\partial}{\partial t} \right) |A_{\omega_2}^\pm|^2 \\ &= -\frac{1}{\kappa_3^\mp} \left(\frac{\partial}{\partial z} + (k'_3 \pm a'_3) \frac{\partial}{\partial t} \right) |A_{\omega_3}^\mp|^2. \end{aligned} \quad (11)$$

This constitutes the Manley–Rowe relation [2] for three-wave mixing involving three pulses, including the reduced transfer rate in cases where the overlap between the idler, signal, and pump pulses is affected by the difference in LCP and RCP group velocities $v_{g_j}^\pm = (k'_j \mp a'_j)^{-1}$.

For numerical purposes, it is convenient to transform the system [Eq. (7)] into a normalized and dimensionless form, using two new variables ζ and s defined as

$$\zeta = |k''_3|z/\tau_0^2, \quad s = (t - k'_3 z)/\tau_0, \quad (12)$$

where τ_0 is the characteristic initial time duration of the pump pulse. The spatial coordinate ζ is here normalized against the dispersion length $L_D = \tau_0^2/|k''_3|$, while the normalized time s is expressed in a reference frame moving at the average group velocity of pump pulses. This way, we describe temporal changes of the signal and idler pulses with respect to the pump pulse. We further define the normalized field envelopes u_j^\pm for the idler, signal, and pump pulses as

$$u_j^\pm = \frac{\tau_0^2}{|k''_3|} \left(\frac{\kappa_1^\pm \kappa_2^\pm \kappa_3^\mp}{\kappa_j^\pm} \right)^{1/2} A_{\omega_j}^\pm, \quad j = 1, 2, 3, \quad (13)$$

and further define the dimensionless phase mismatch related to the normalized spatial coordinate ζ as

$$\Delta\phi_\pm = (\Delta k \pm \Delta\alpha) \tau_0^2 / |k''_3|. \quad (14)$$

With the preceding set of parameters and variables, Eq. (7) is transformed into the normalized and dimensionless form:

$$\begin{aligned} & \left(\frac{\partial}{\partial \zeta} + \frac{(k'_1 \mp a'_1 - k'_3) \tau_0}{|k''_3|} \frac{\partial}{\partial s} + i \frac{(k'_1 \mp a'_1)}{2|k''_3|} \frac{\partial^2}{\partial s^2} \right) u_1^\pm \\ &= i u_3^\mp u_2^{\pm*} \exp(i\Delta\phi_\pm \zeta), \end{aligned} \quad (15a)$$

$$\begin{aligned} & \left(\frac{\partial}{\partial \zeta} + \frac{(k'_2 \mp a'_2 - k'_3) \tau_0}{|k''_3|} \frac{\partial}{\partial s} + i \frac{(k'_2 \mp a'_2)}{2|k''_3|} \frac{\partial^2}{\partial s^2} \right) u_2^\pm \\ &= i u_3^\mp u_1^{\pm*} \exp(i\Delta\phi_\pm \zeta), \end{aligned} \quad (15b)$$

$$\begin{aligned} & \left(\frac{\partial}{\partial \zeta} \pm \frac{a'_3 \tau_0}{|k''_3|} \frac{\partial}{\partial s} + i \frac{(k'_3 \pm a'_3)}{2|k''_3|} \frac{\partial^2}{\partial s^2} \right) u_3^\mp \\ &= i u_1^\pm u_2^\pm \exp(-i\Delta\phi_\pm \zeta). \end{aligned} \quad (15c)$$

In this form, the first-order temporal derivative term in the equation for the pump results from group-velocity gyrotropy. Whenever $a'_3 \neq 0$ in Eq. (15c), the two circularly polarized components of the pump pulse travel with different group velocities inside the chiral medium. As a result, these two components, although overlapping perfectly before entering the medium, separate from each other, which, for large distances of propagation, will separate the RCP or LCP components spatially, affecting the OPA process.

As for the corresponding Manley–Rowe relations [Eq. (11)], in the normalized space and time coordinates, following the pump pulse, they yield

$$\begin{aligned} & \left(\frac{\partial}{\partial \zeta} + \frac{(k'_1 \mp a'_1 - k'_3) \tau_0}{|k''_3|} \frac{\partial}{\partial s} \right) u_1^\pm \\ &= \left(\frac{\partial}{\partial \zeta} + \frac{(k'_2 \mp a'_2 - k'_3) \tau_0}{|k''_3|} \frac{\partial}{\partial s} \right) u_2^\pm \\ &= - \left(\frac{\partial}{\partial \zeta} \pm \frac{a'_3 \tau_0}{|k''_3|} \frac{\partial}{\partial s} \right) u_3^\mp. \end{aligned} \quad (16)$$

In these relations for energy transfer, the coefficients of the normalized temporal derivatives express the effects of walk-off of the idler ($k'_1 - k'_3$) and signal ($k'_2 - k'_3$) pulses relative to the pump, including the differential effect of gyrotropy ($\mp a'_j$).

4. NUMERICAL RESULTS

The set of coupled nonlinear and partial differential equations [Eq. (15)] can be solved with the well-known split-step Fourier method [15,16], using the matrix formulation

$$\frac{\partial \mathbf{u}_\pm(\zeta, s)}{\partial \zeta} = (\mathbb{D}_\pm + i\mathbb{N}_\pm) \mathbf{u}_\pm(\zeta, s), \quad (17)$$

where $\mathbf{u}_\pm = (u_1^\pm, u_2^\pm, u_3^\mp)^T$, and \mathbb{D}_\pm and \mathbb{N}_\pm are the two $[3 \times 3]$ matrices

$$\mathbb{D}_\pm = \begin{pmatrix} D_1^\pm & 0 & 0 \\ 0 & D_2^\pm & 0 \\ 0 & 0 & D_3^\mp \end{pmatrix}, \mathbb{N}_\pm = \begin{pmatrix} 0 & 0 & N_2^\pm \\ 0 & 0 & N_1^\mp \\ 0 & N_1^{\pm*} & 0 \end{pmatrix}, \quad (18)$$

with operators in normalized time

$$D_j^\pm = -\frac{(k'_j \mp a'_j - k'_3)\tau_0}{|k'_3|} \frac{\partial}{\partial s} - i \frac{(k''_j \mp a''_j)}{2|k'_3|} \frac{\partial^2}{\partial s^2} \quad (19)$$

and

$$N_j^\pm = u_j^{\pm*}(\zeta, s) \exp(i\Delta\phi_\pm\zeta). \quad (20)$$

The diagonal operator $\mathbb{D}_\pm = \mathbb{D}_\pm(\partial/\partial s)$, taking care of all dispersive effects, is applied in the Fourier domain, conjugate of normalized time, where $\partial/\partial s \rightarrow -i\omega_j$ becomes an imaginary number. The off-diagonal matrix $\mathbb{N}_\pm = \mathbb{N}_\pm(\mathbf{u}_\pm)$, governing the nonlinear effects, is applied most easily in the ζ space.

In order to solve Eq. (17), we need to specify the dispersion and chiral parameters of the medium appearing in Eq. (15) at the wavelengths of the idler, signal, and pump pulses. Keeping in mind a trigonal chiral crystal of point-symmetry group 32, the group velocities of the three pulses are taken to be $0.99/k'_1 = 0.99/k'_2 = 1/k'_3 = 2.0 \times 10^8$ m/s so that they travel at nearly the same speed and keep overlapping within the chiral crystal. The dispersion coefficients for the group velocity are assumed to be the same for three pulses, with the value $k''_j = 10.0 \times 10^{-21} s^2/\text{m}$ for $j = 1, 2, 3$. Chiral corrections to these coefficients are chosen as $a'_j = 3.0 \times 10^{-4} k'_j$ and $a''_j = 0$. We also need to specify the phase-mismatch associated with the OPA process, consisting of two parts. We chose $\Delta k = 0$ for the electric dipolar part and $\Delta\alpha = 400.0 \text{ m}^{-1}$ for the chiral part to illustrate the importance of chiral phase matching. The preceding parameter values are reasonable for qualitative discussion, but they do not correspond to an actual experiment.

We also need to specify the pump and signal pulses that would be launched into the crystal in any OPA experiment. Again, both the shape and width of pulses can vary from experiment to experiment. We chose sech-shape for both pulses with an initial full-width at half maximum of $\tau_0 = 10$ ps. We also assume both pulses to be linearly polarized initially and excite the LCP and RCP components inside the chiral crystal with the same amplitude. The normalized peak amplitude of the pump pulses depends on the nonlinear coupling parameters, as shown in Eq. (13), and should be high enough to amplify the signal pulse considerably. Mathematically, the chosen initial conditions for the signal and pump at $\zeta = 0$, used for solving Eq. (15), are

$$u_2^\pm(0, s) = 0.5 \text{ sech } s, \quad u_3^\pm(0, s) = 2.5 \text{ sech } s, \quad (21)$$

together with $u_1^\pm(0, s) = 0$. The differential phase-matching condition creates a differential contribution to the LCP and RCP coherence lengths $L_C^\pm = \pi/(\Delta k \pm \Delta\alpha)$, from which the beat length between subsequent points of equal phase-matching conditions for the LCP and RCP modes is obtained as $L_B = \pi/(2\Delta\alpha)$.

The OPA process in a chiral nonlinear crystal is known to modify the state of polarization (SOP) of the three waves while

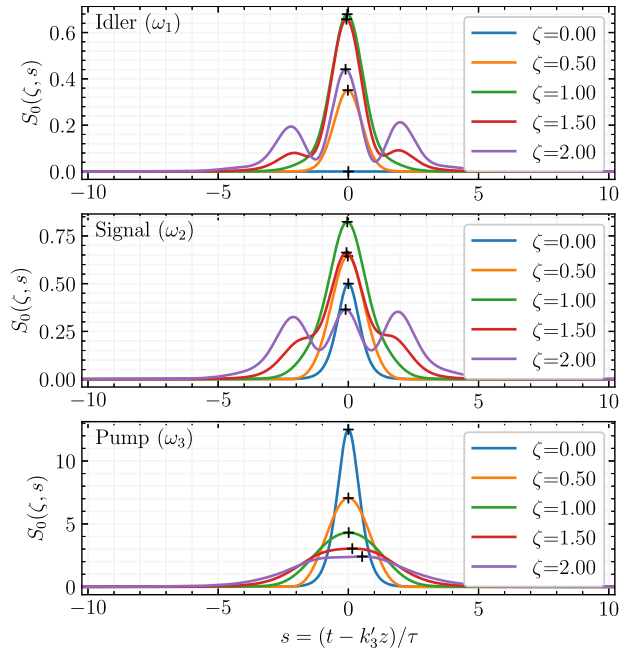


Fig. 1. Intensity profiles of the idler, signal, and pump pulses at several distances within the chiral crystal used for OPA; $\zeta = 1$ corresponds to a distance of about 1 cm for the parameters used here.

transferring energy from the pump to the signal and idler [14]. In the case of pulsed OPA, we expect the SOP to also become nonuniform across each pulse. To quantify such polarization changes, we make use of the Stokes parameters of the idler, signal, and pump waves defined as [17]

$$\begin{aligned} S_{0j} &= |u_j^+|^2 + |u_j^-|^2, & S_{1j} &= 2\text{Re}[u_j^{+*} u_j^-], \\ S_{3j} &= |u_j^+|^2 - |u_j^-|^2, & S_{2j} &= 2\text{Im}[u_j^{+*} u_j^-], \end{aligned} \quad (22)$$

where S_{3j}/S_{0j} provides the ellipticity of the polarization ellipse for $j = 1, 2, 3$. Notice that $S_{0j}(s)$ provides the total normalized power at time s for each pulse. Using its definition, the pump's peak power is 25 times larger than the signal's peak power for the input choice in Eq. (21).

Figure 1 shows the evolution of idler, signal, and pump pulses by plotting their total intensity S_{0j} ($j = 1, 2, 3$) as a function of normalized time at several distances within the chiral crystal, with the curves at $\zeta = 0$ showing the initial shape of pulses. The corresponding SOP changes are shown in Fig. 2, where the ellipticities S_{3j} are mapped as a function of time. As expected, energy is transferred from the pump pulse to the signal pulse while also generating an idler pulse. While the pump pulse broadens because of group velocity dispersion inside the crystal, the idler and signal pulses develop a three-peak structure after $\zeta = 1$, a value that corresponds to a distance of about 1 cm for the parameters used here. The origin of this structure lies in slightly different group velocities of the signal and idler compared to the pump pulse, whose LCP and RCP components also travel at different speeds. Different parts of the signal and idler pulses overlap with the pump components and create two side peaks, in addition to the original central peak at $s = 0$. At a distance $\zeta = 2$, the three peaks of the signal pulse have comparable amplitudes. Splitting of the original signal pulse into a triplet

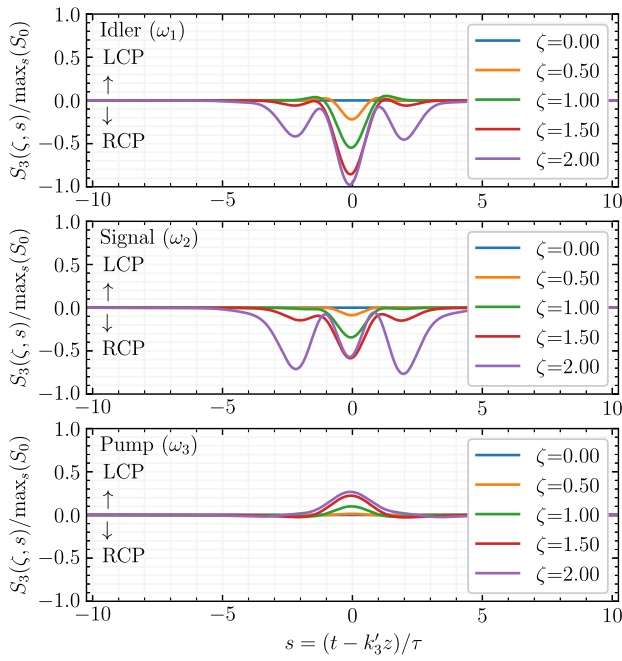


Fig. 2. Same as Fig. 1, except that the ellipticity of the SOP, normalized against the peak intensity of the pulse, is mapped as a function of s at the same five distances.

effectively depends on the temporal separation introduced by different group velocities of the LCP and RCP modes over the coherence length L_C , with consideration taken for the pulse broadening imposed by the group velocity dispersion. This process provides an efficient energy transfer from the pump to the signal while allowing the LCP and RCP modes to slip out of the spatial coverage of the pump pulse, effectively stopping the parametric interaction as soon as the triplet has been formed.

The results shown in Fig. 2 clearly indicate that the initially linear SOP of the pump and signal pulses quickly change to elliptical ones due to the effects of chirality. What is remarkable is that the SOP also becomes different across the temporal profile of both pulses. The pump's ellipticity remains small and exhibits a single peak at the pulse's center. In contrast, the ellipticity of the signal and idler pulses mimics the three-peak structure of the shape of these pulses. Combined with the possibility of tuning the signal's wavelength, this rapid modulation of the SOP opens a new direction for measuring the orbital and spin angular momenta in pump-probe experiments.

The preceding results for 10 ps wide pump pulses yield a relatively short equivalent Gaussian dispersion length of $L_D = \tau_0^2 / |k_j''| = 10$ mm, a distance over which the temporal walk-off between the LCP and RCP modes due to different group velocities is relatively small, as is also the group velocity mismatch between the idler, signal, and pump. We next consider the situation where the group velocity mismatch dominates over dispersion-induced pulse broadening. We keep all parameters the same except for the following changes. First, the pump and signal pulses are shortened to yield a FWHM duration of $\tau_0 = 0.5$ ps, and we allow a lower dispersion of $k_j'' = 1.0 \times 10^{-23}$ s²/m, resulting in a dispersion length of

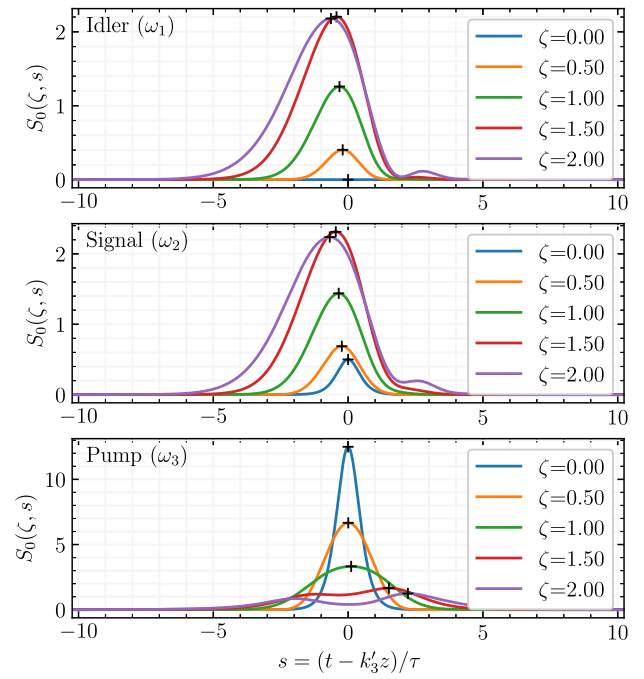


Fig. 3. Intensity profiles of the idler, signal, and pump pulses mapped at several distances for the case in which polarization-mode dispersion dominates over the temporal walk-off effects.

$L_D = 25$ mm. Second, we assume a slightly lower difference in group velocity $0.9975/k_1' = 0.9975/k_2' = 1/k_3' = 2.0 \times 10^8$ m/s, with associated chiral parameters $a_j' = 2.0 \times 10^{-3} k_j'$ for $j = 1, 2, 3$, being larger by a factor of 7 compared to the earlier results. Again, for the sake of illustration of principle, we chose $\Delta k = 0$ for the electric dipolar part, but reduced the chiral differential contribution to $\Delta\alpha = 50.0$ m⁻¹.

It should be noted that the values of k'' differ considerably for the long and short pulses used for numerical simulations. For any dispersive chiral crystal (or liquid), k'' would be zero at a specific wavelength, known as the zero-dispersion wavelength. In practice, the wavelength of a pump laser can be chosen close to or far from the zero-dispersion wavelength of the chiral medium to realize different values of the parameter k'' . As the zero-dispersion wavelength of a chiral medium is expected to vary with the choice of the chiral crystal, the pump's wavelength may also vary over a wide range from the visible to the near-infrared region.

The solutions to Eq. (17) under these altered conditions are shown in Figs. 3 and 4. As previously, the signal pulse broadens as it is amplified, but it does not split into three parts; instead, a remarkable fast intrapulse flipping of the SOP of the three pulses occur, as demonstrated in Fig. 4. As seen there, the elliptical SOP flips between the LCP and RCP states over the duration of all three pulses. Again, this process is a result of a large temporal overlap between the pump and signal pulses during parametric interaction. Even though the LCP and RCP signal pulses slip relative to each other during this interaction over a coherence length L_C , they keep overlapping sufficiently in this specific case with a lower pulse broadening.

Depending on the magnitude of the group-velocity difference $\Delta v_{gj} = 2a_j' / (k_j'^2 - a_j'^2)$ and the circular birefringence

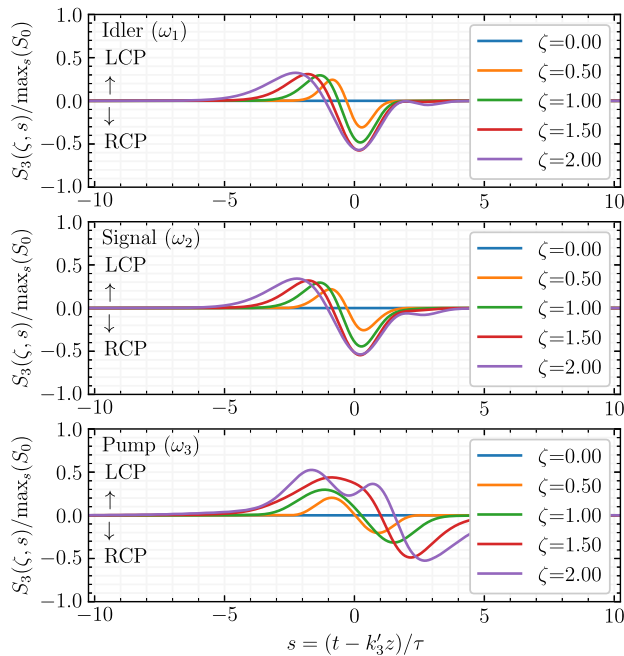


Fig. 4. Same as Fig. 3, except that ellipticity of the SOP is mapped as a function of s at the same five distances.

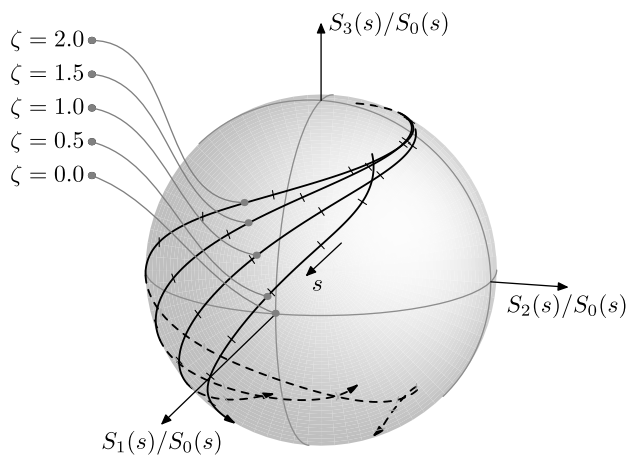


Fig. 5. SOP trajectories of the normalized Stokes parameters ($S_1(s)$, $S_2(s)$, $S_3(s)$)/ $S_0(s)$ for the signal pulse as a function of normalized time s , relative to the inertial frame of the pump pulse, mapped onto the Poincaré sphere covering the duration of a signal pulse at five normalized distances in the range from $\zeta = 0$ to 2, in the same configuration as in Figs. 3 and 4.

$\Delta\alpha$, intrapulse polarization state flipping may take a straight or helicoidal path on the Poincaré sphere. This is illustrated in Fig. 5, where the SOP changes across the signal pulse are displayed on the Poincaré sphere at the same five distances. The SOP trajectories for the signal pulse make use of the Stokes parameters ($S_1(s)$, $S_2(s)$, $S_3(s)$)/ $S_0(s)$ that depend on the normalized time s . The trajectories in Fig. 5 are extracted as the segments in normalized time s covering the span in which the signal intensity $S_0(s)$ exceeds one percent of its maximum value for each value of ζ . Recalling that $\zeta = 1$ corresponds to a distance of propagation of 25 mm, the results shown in Figs. 3–5

are applicable to low-dispersive waveguides doped with a chiral nonlinear material.

5. CONCLUSION

In this work, we have shown how chirality affects the OPA process in a nonlinear optical medium when the pump, signal, and idler waves are launched in the form of optical pulses. A set of six coupled nonlinear equations was derived for the circularly polarized components of the pump, signal, and idler pulses, after including both the electric dipolar and nonlocal contributions to the linear and nonlinear susceptibilities of the medium. Our equations for wave propagation include differential group delay and group-velocity dispersion induced by the chirality of the medium. Numerical solutions to the pulsed OPA process in a chiral crystal reveal novel features such as a three-peak structure of the signal and idler pulses and fast intrapulse flipping of their polarization states.

We have also demonstrated the possibility of employing the chirality of a nonlinear medium for differential phase matching between orthogonal circular polarization states, with the beat length determining the period of alternating and recurring conditions between the polarization states for parametric generation. The Manly–Rowe relations for the pulsed nonlinear process show the interplay between the polarization state and group-velocity deviations between the quasi-monochromatic fields, including the resulting differential walk-off effects between LCP and RCP modes.

In cases where the pulse duration of the signal is significantly different from that of the pump pulse, the flanks of the signal will act as seeds for starting the parametric process of energy transfer. However, a strong signal peak within the regime of efficient phase-matching will cut a significant portion of its overlap with the pulse. In this respect, the chirality will have the impact of a differential sliding overlap for the LCP and RCP modes, resulting in pulses with circular polarization states of different polarity on their leading and trailing flanks. This fast intrapulse flipping between the two circular polarization states suggests spintronic pump and probe experiments, where fast switching of a frequency-tuned signal may be used in conjunction with another light source as a pump.

Disclosures. The authors declare no conflicts of interest.

Data availability. Data underlying the results presented in this article are not publicly available at this time but may be obtained from the authors upon reasonable request.

REFERENCES

1. R. M. Baumgartner and R. L. Byer, "Optical parametric amplification," *IEEE J. Quantum Electron.* **15**, 432–444 (1979).
2. Y. R. Shen, *The Principles of Nonlinear Optics* (Wiley, 1984).
3. B. Busson, M. Kauranen, C. Nuckolls, *et al.*, "Quasiphase-matching in chiral materials," *Phys. Rev. Lett.* **84**, 79–82 (2000).
4. S. Witte and K. S. E. Eikema, "Ultrafast optical parametric chirped-pulse amplification," *IEEE J. Quantum Electron.* **18**, 296–307 (2012).
5. E. Ibragimov, A. Struthers, and D. J. Kaup, "Soliton pulse compression in the theory of optical parametric amplification," *Opt. Commun.* **152**, 101–107 (1998).
6. P. P. Bey and H. Rabin, "Coupled-wave solution of harmonic generation in an optically active medium," *Phys. Rev.* **162**, 794–800 (1967).

7. F. Jonsson and C. Flytzanis, "Optical parametric generation and phase matching in magneto-optic media," *Opt. Lett.* **24**, 1514–1516 (1999).
8. F. Jonsson and C. Flytzanis, "Photospin-orbit coupling in photonic structures," *Phys. Rev. Lett.* **97**, 193903 (2006).
9. C. Flytzanis, *Theory of Nonlinear Optical Susceptibilities* (Academic, 1975), Vol. I, Part A, pp. 9–207.
10. I. C. Khoo, "Extreme nonlinear optics of nematic liquid crystals," *J. Opt. Soc. Am. B* **28**, A45–A55 (2011).
11. I. C. Khoo, C.-W. Chen, T.-M. Feng, *et al.*, "Nonlinear liquid crystalline chiral photonic crystals for visible to mid-infrared optical switching and modulation," in *Optica Nonlinear Optics Topical Meeting* (Optica Publishing Group, 2023), paper Tu1B.3.
12. D. Xue and S. Zhang, "Calculations of nonlinear optical responses of isomorphous crystals NaClO_3 and NaBrO_3 with natural optical activity," *Chem. Phys. Lett.* **287**, 503–508 (1998).
13. M. Karppinen, "Origin of optical activity in cubic NaClO_3 and NaBrO_3 crystals at 296K," *Eur. J. Appl. Sci.* **12**, 174–184 (2024).
14. C. Flytzanis, F. Jonsson, and G. P. Agrawal, "Optical parametric amplification and oscillation in nonlinear chiral media," *J. Chem. Phys.* **161**, 184110 (2024).
15. G. P. Agrawal, *Nonlinear Fiber Optics*, 2nd ed. (Academic, 1995), Section 2.4.1.
16. R. Deiterding, R. Glowinski, H. Oliver, *et al.*, "A reliable split-step Fourier method for the propagation equation of ultra-fast pulses in single-mode optical fibers," *J. Lightwave Technol.* **31**, 2008–2017 (2013).
17. M. Born and E. Wolf, *Principles of Optics*, 7th ed. (Cambridge University, 1999).